Observation of momentum-dependent charge excitations in hole-doped cuprates using resonant inelastic x-ray scattering at the oxygen K edge

Kenji Ishii,[1] Takami Tohyama,[2] Shun Asano,[3] Kentaro Sato,[3] Masaki Fujita,[3] Shuichi Wakimoto,[4] Kenji Tustsui,[1] Shigetoshi Sota,[5] Jun Miyawaki,[6] Hideharu Niwa,[6] Yoshihisa Harada,[6] Jonathan Pelliciari,[7,*] Yaobo Huang,[7] Thorsten Schmitt,[7] Yoshiya Yamamoto,[8] and Jun'ichiro Mizuki[8]

[1]*Synchrotron Radiation Research Center, National Institutes for Quantum and Radiological Science and Technology, Hyogo 679-5148, Japan*
[2]*Department of Applied Physics, Tokyo University of Science, Tokyo 125-8585, Japan*
[3]*Institute for Materials Research, Tohoku University, Sendai 980-8577, Japan*
[4]*Materials Sciences Research Center, Japan Atomic Energy Agency, Ibaraki 319-1195, Japan*
[5]*Computational Materials Science Research Team, RIKEN Advanced Institute for Computational Science (AICS), Kobe, Hyogo 650-0047, Japan*
[6]*Institute for Solid State Physics, University of Tokyo, Chiba 277-8581, Japan*
[7]*Research Department Synchrotron Radiation and Nanotechnology, Paul Scherrer Institut, CH-5232 Villigen PSI, Switzerland*
[8]*Graduate School of Science and Technology, Kwansei Gakuin University, Hyogo 669-1337, Japan*

We investigate electronic excitations in $La_{2-x}(Br,Sr)_xCuO_4$ using resonant inelastic x-ray scattering (RIXS) at the oxygen K edge. RIXS spectra of the hole-doped cuprates show clear momentum dependence below 1 eV. The broad spectral weight exhibits positive dispersion and shifts to higher energy with increasing hole concentration. Theoretical calculation of the dynamical charge structure factor on oxygen orbitals in a three-band Hubbard model is consistent with the experimental observation of the momentum and doping dependence, and therefore the momentum-dependent spectral weight is ascribed to intraband charge excitations which have been observed in electron-doped cuprates. Our results confirm that the momentum-dependent charge excitations exist on the order of the transfer energy (t), and the broad spectral line shape indicates damped and incoherent character of the charge excitations at the energy range in the doped Mott insulators.

I. INTRODUCTION

Strongly correlated transition-metal oxides display various interesting physical properties, including metal-insulator transition, high-temperature superconductivity, and colossal magnetoresistance, and some of the oxides are classified into doped Mott insulators where electron correlation significantly modifies their band structure, which diverges from that of the noninteracting simple metal [1]. Among the doped Mott insulators, superconducting cuprates are most intensively studied [2]. This is mainly due to the superconductivity at the high transition temperature and related phenomena such as pseudogap and a competing phase with charge order [3]. In addition to the interest of superconductivity, doped cuprates are important and suitable for the study of the electronic structure of the doped Mott insulator because relatively simple theoretical models with a few orbitals are applicable to describe the electronic structure near the Fermi energy. They represent the benchmark of the doped Mott insulators, and the clarification of the fundamental electronic structure is essential for understanding the mechanism of the physical phenomena in the doped cuprates.

In the undoped cuprates, only the spin degree of freedom contributes to the low-energy electron dynamics. When carriers are doped, the charge degree of freedom becomes active and the electron dynamics is characterized by the motion of spin and charge. Therefore, we consider that both spin and charge excitations must be investigated on equal footing in order to understand the electron dynamics characterizing the physics of the cuprates. Inelastic neutron scattering (INS) has been widely used for studying the spin dynamics in the reciprocal lattice space, and high-resolution resonant inelastic x-ray scattering (RIXS) at the Cu L_3 edge has recently become an alternative to measure momentum-resolved spin excitations up to several hundred meV [4,5]. Charge excitations in the doped cuprates extend to higher energy than the spin excitations, and the electron correlation affects the charge excitations of the order of a few electronvolts. Optical studies [6,7] demonstrated that the spectral weight of the intraband charge excitations emerges below the charge-transfer gap in the doped cuprates, and the weight characterizes the charge excitations in the doped Mott insulators. The high-energy part of momentum-resolved charge excitations below the gap was studied by Cu K-edge RIXS [8–10], but the huge tail of the elastic scattering hampers the observation below several hundred meV. Alternatively, the capability of Cu L_3-edge RIXS for the detection of the charge excitations is argued theoretically [11,12], and particle-hole charge excitations have been reported in a Ti L_3-edge RIXS study on the weakly correlated broadband material $1T$-TiSe$_2$ [13]. Nevertheless, momentum-dependent charge excitations in the hole-doped cuprates, to the best of our knowledge, have not been identified experimentally using Cu L_3-edge RIXS. On the other hand, in electron-doped cuprates, a dispersive mode which is located at higher energy than the spin excitations was found in the Cu L_3-edge RIXS spectra [14,15] and it is ascribed to the particle-hole charge excitations [14]. However, the origin of this mode is still controversial.

*Present address: Department of Physics, Massachusetts Institute of Technology, Cambridge, Massachusetts 02139, USA.
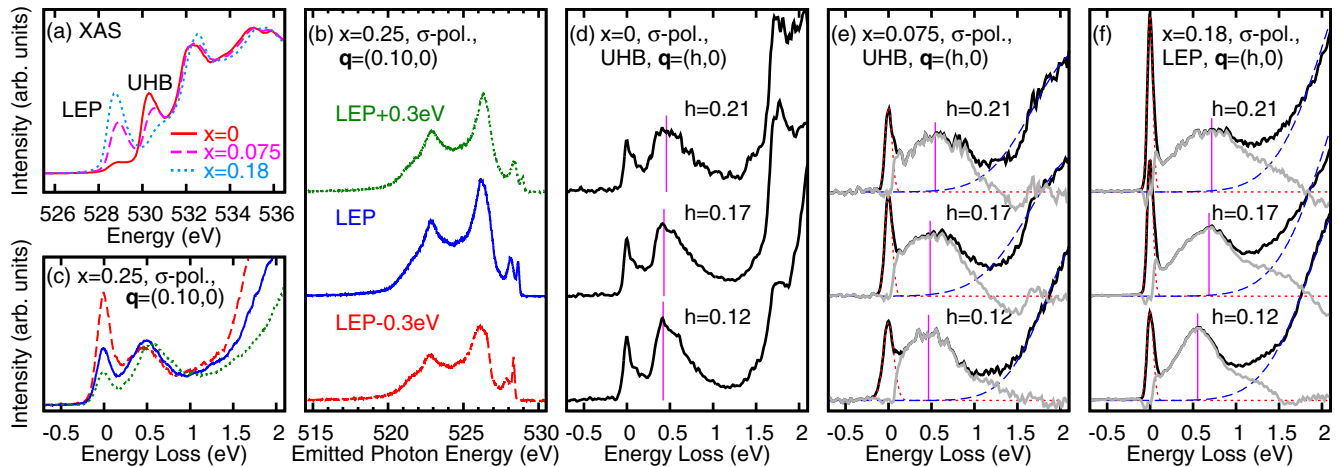
FIG. 1. (a) X-ray absorption spectra near the oxygen K edge. X-ray polarization is parallel to the CuO$_2$ plane. (b) O K-edge RIXS spectra of La$_{2-x}$Sr$_x$CuO$_4$ ($x = 0.25$) plotted against emitted photon energy. From bottom to top, the incident photon energy is tuned to LEP $- 0.3$ eV, LEP, and LEP $+ 0.3$ eV of XAS. (c) The same spectra as in (b) plotted as a function of energy loss. (d–f) RIXS spectra of La$_{2-x}$Sr$_x$CuO$_4$. The energy of the σ-polarized incident x rays is tuned to UHB for $x = 0$ (d) and $x = 0.075$ (e) and LEP for $x = 0.18$ (f). Black lines are the raw spectra and gray lines in (e) and (f) are the spectral weight after subtraction of the elastic peak (dotted line) and high-energy tail (dashed line). The vertical bars indicate the peak position of the spectral weight after subtraction.

In Ref. [15], a different interpretation that is associated with a symmetry-breaking state other than superconductivity is proposed, and this dispersive mode is considered to be absent in hole-doped cuprates. Furthermore, it is discussed in a theoretical study [16] that the dispersive mode comes from a plasmon excitation. In order to settle this controversy, it is necessary to confirm whether such a dispersive mode exists also in hole-doped cuprates.

In this paper, we report that momentum-dependent charge excitations in the hole-doped cuprates can be observed using O K-edge RIXS. The experimental observation of the momentum and doping dependence is consistent with a theoretical calculation of the dynamical charge structure factor on oxygen orbitals in a three-band Hubbard model with Cu $3d_{x^2-y^2}$ and two O $2p_\sigma$ orbitals. Therefore we ascribe the dispersive mode to intraband charge excitations. Our result demonstrates that the intraband charge excitations are qualitatively symmetric between the hole- and electron-doped cuprates.

II. EXPERIMENTAL DETAILS

The RIXS experiments were performed using the SAXES spectrometer [17] at the ADRESS beam line [18] of the Swiss Light Source (SLS) at the Paul Scherrer Institut and the HORNET spectrometer [19] at beam line BL07LSU [20] of SPring-8. The RIXS spectra in Figs. 1(d)–1(f) were taken at the former and others were measured at the latter, with respective energy resolutions of 60 and 170–190 meV. The scattering angle (2θ) was set to 130° for Figs. 1(d)–1(f), 90° for Figs. 2(a) and 2(d), and 135° for Figs. 1(b) and 1(c) and Figs. 2(b), 2(c) and 2(e). Single crystals of La$_{2-x}$Sr$_x$CuO$_4$ (LSCO with $x = 0, 0.075, 0.18$, and 0.25) and La$_{2-x}$Ba$_x$CuO$_4$ (LBCO with $x = 0.125$) were measured at the base temperature of sample manipulators (10–30 K). At $x = 0.125$, substitution of Sr and Ba for La has a different effect on the physical properties, including charge order and superconductivity [21]. However, as shown later, the charge excitations discussed in this paper

do not change at the charge order La$_{2-x}$Ba$_x$CuO$_4$ ($x = 0.125$), and the energy scale of superconductivity (<100 meV) is lower than the energy range discussed in this paper. Therefore the difference of the alkaline earth metals is irrelevant for the present study, and we can distinguish the samples by mere hole concentration (x). The crystals were cleaved before the measurement, and σ-polarized x rays were irradiated on the ab plane of the crystals. The c axis was kept parallel to the horizontal scattering plane, and momentum transfer in the CuO$_2$ plane (**q**) was scanned by rotating the crystal along the vertical axis.

In the x-ray absorption spectrum (XAS) of the doped cuprates, two peaks are observed near the O K edge [22]. As shown in Fig. 1(a), the spectral weight of the transition to the upper Hubbard band (UHB) transfers to the lower-energy peak (LEP) with increasing the hole concentration. The incident photon energy for the RIXS measurements was tuned to the top of either the LEP or UHB of the respective samples. In the undoped $x = 0$, large enhancement of excitations is observed only at the UHB resonance. When holes are doped to $x = 0.075$, the spectral weight of XAS becomes comparable between LEP and UHB. We measured the RIXS spectra at both LEP and UHB resonances, but, as shown in Figs. 2(a) and 2(f), we could not find any significant difference at the sub-eV range between the two resonance conditions. Because the spectral weight of LEP is dominant in XAS for higher doping ($x = 0.125, 0.18$, and 0.25), we took the RIXS spectra at the LEP resonance.

III. EXPERIMENTAL RESULTS

Figure 1(b) shows the incident photon energy (E_i) dependence near LEP for $x = 0.25$. The spectral shape is almost unchanged below 527 eV, meaning that most of the spectral weight in this energy region comes from fluorescence. The spectra discussed below are normalized to the integrated intensity of the fluorescence. In Fig. 1(c) we plot the same
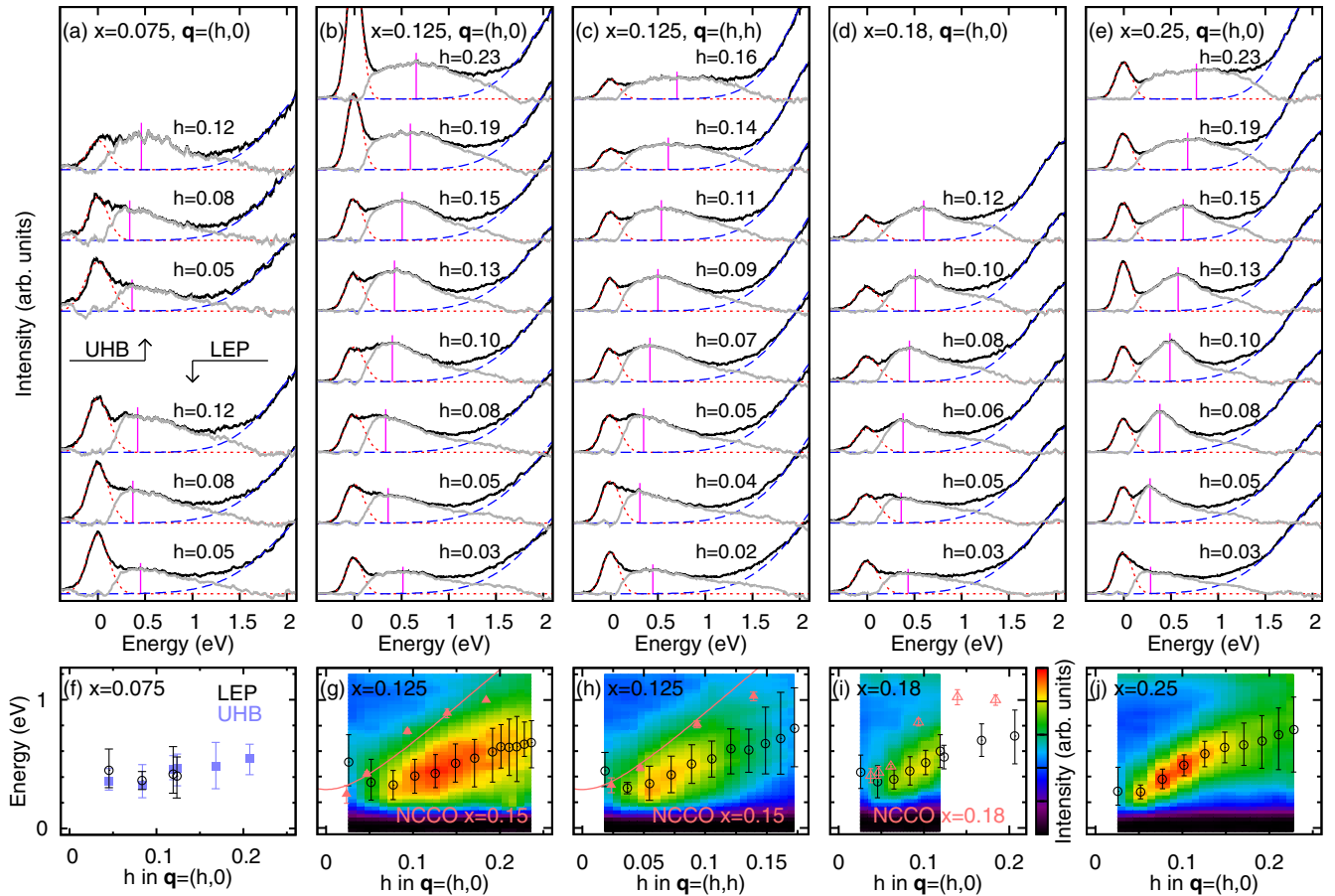
FIG. 2. (a–e) RIXS spectra of $La_{2-x}(Br,Sr)_xCuO_4$. The energy of the σ-polarized incident x-rays is tuned to LEP of XAS, except for the upper three spectra in (a). Black lines are the raw spectra, and gray lines are the spectral weight after subtraction of the elastic peak (dotted line) and high-energy tail (dashed line). The peak position is taken to be the centroid within the region where the spectral intensity exceeds 90% of maximum in the subtracted spectrum and indicated by the vertical bar. (f–j) Dispersion relation of the dispersive mode. Peak positions are plotted by open circles and filled squares. Full widths at 90% of the maximum intensity are displayed by vertical bars. Results from the spectra in Figs. 1(c) and 1(d) are included. In (g–j), RIXS intensity of (b–e) is displayed as a color map after subtracting the elastic component. Peak positions of the charge excitations [14] and the fast-dispersive mode [15] in electron-doped $Nd_{2-x}Ce_xCuO_4$ are also shown by triangles and solid lines, respectively.

spectra as in Fig. 1(b) as a function of energy loss. The spectral weight at around 0.5 eV slightly shifts to higher energy with increasing E_i, indicating a nonperfect Raman behavior, but the shift is much smaller than the variation of E_i.

Figures 1(d)–1(f) show the momentum dependence of the O K-edge RIXS spectra for $x = 0$, 0.075, and 0.18, respectively. On subtracting the elastic peak and the high-energy tail, it is possible to identify a broad peaked feature below 1 eV in all three samples. Position and line shape of the peaked feature of the undoped compound ($x = 0$) are independent of $\mathbf{q}$ and it is ascribed to two-magnon excitations [23,24]. In contrast, the energy position of the peaked feature of $x = 0.075$ and 0.18 changes with momentum. The qualitative difference of the momentum dependence indicates that another type of excitation exists in the spectra of the doped compounds.

For the doped compounds, we measured the RIXS spectra in a finer interval of momentum and summarize them in Figs. 2(a)–2(e). We subtract the elastic scattering and high-energy tail from the raw spectra and plot the peak positions of residual intensity (gray lines) as a function of $\mathbf{q}$ in Figs. 2(f)–2(j). Because systematic fitting analysis is difficult due to

the strongly momentum-dependent line shape, a centroid within the region where the spectral intensity exceeds 90% of the maximum in the residual is taken as the peak position. RIXS intensity after subtracting the elastic scattering is also displayed as color maps in Figs. 2(g)–2(j). Except for the close vicinity of $\mathbf{q} = (0,0)$, the spectral weight at the sub-eV region shifts to higher energy with increasing momentum transfer, showing positive dispersion. The magnitude of the dispersion of the mode becomes larger with increasing hole concentration. For example, the peak position at $\mathbf{q} = (0.23,0)$ is 0.66 eV for $x = 0.125$ while it is 0.77 eV for $x = 0.25$. Comparing the spectral weights at the same $|\mathbf{q}|$ of $x = 0.125$, the peak of the (h,h) direction is located at higher energy than that of the $(h,0)$ direction.

In a published work on LSCO, the peak at the sub-eV region in the O K-edge RIXS spectra was ascribed to two-magnon excitations, not only for the undoped compound but also for the doped ones [24,25]. We do not exclude the possibility that a part of the spectral weight of the doped compounds comes from two-magnon excitations, but the momentum-dependent excitations should have another origin for the following

reasons. First, the energy of the peak positions is too high to ascribe the momentum-dependent excitations to two magnons. The excitation energy at large **q** in the present measurements is 0.6–0.8 eV while calculated two-magnon density of states for a nearest-neighbor Heisenberg antiferromagnet with exchange interaction J is located lower than $4J \simeq 0.5$ eV [26]. Secondly, in Raman scattering studies [27–30], the energy of two-magnon excitations rapidly decreases upon hole doping, in contrast with our experimental fact that the peak of the momentum-dependent excitations at large **q** shifts to higher energy with increasing hole concentration. Third, the peak becomes salient in the overdoped compound ($x = 0.25$), which is situated farthest from the antiferromagnetic ordered phase. Finally, theoretical calculations of two-magnon excitations in a hole-doped t-J-type model show negligible **q** dependence (see Appendix A). All of these facts suggest that two-magnon excitations are not the origin of the momentum-dependent excitations.

IV. THEORETICAL CALCULATION

In order to identify the origin of the dispersive mode, we perform theoretical calculations of the dynamical charge structure factor on oxygen orbitals in a three-band Hubbard model for the CuO$_2$ plane. Three-band Hubbard Hamiltonian is given by

$$
\begin{aligned}
H = \sum_{i,\sigma} [& T_{pd} d^\dagger_{i,\sigma} (p_{i+\mathbf{y},\sigma} - p_{i+\mathbf{x},\sigma} - p_{i-\mathbf{y},\sigma} + p_{i-\mathbf{x},\sigma}) \\
& + T_{pp} (p^\dagger_{i+\mathbf{y},\sigma} p_{i+\mathbf{x},\sigma} - p^\dagger_{i-\mathbf{x},\sigma} p_{i+\mathbf{y},\sigma} \\
& + p^\dagger_{i-\mathbf{y},\sigma} p_{i-\mathbf{x},\sigma} - p^\dagger_{i+\mathbf{x},\sigma} p_{i-\mathbf{y},\sigma}) + \text{H.c.}] \\
& + \Delta \sum_{i,\delta,\sigma} n^p_{i+\delta,\sigma} + U_d \sum_i n^d_{i,\uparrow} n^d_{i,\downarrow} + U_p \sum_{i,\delta} n^p_{i+\delta,\uparrow} n^p_{i+\delta,\downarrow},
\end{aligned}
$$

where the operator $d_{i,\sigma}$ annihilates holes with spin σ in the $3d_{x^2-y^2}$ orbital at site i, $n^d_{i,\sigma} = d^\dagger_{i,\sigma} d_{i,\sigma}$, the $p_{i\pm\mathbf{x(y)},\sigma}$ are the hole annihilation operators for the $2p_x$ ($2p_y$) orbitals at site $i \pm \mathbf{x(y)}$, **x** (**y**) being the vector connecting neighboring Cu and O ions along the x (y) directions, δ is either **x** or **y**, and $n^p_{i+\delta,\sigma} = p^\dagger_{i+\delta,\sigma} p_{i+\delta,\sigma}$. T_{pd} is the hopping between Cu $3d_{x^2-y^2}$ and O $2p_\sigma$ orbitals, T_{pp} is the hopping between neighboring O $2p_\sigma$ orbitals, Δ is the charge-transfer energy between Cu $3d_{x^2-y^2}$ and O $2p_\sigma$ orbitals, U_d is the on-site Coulomb interaction on Cu $3d_{x^2-y^2}$, and U_p is the on-site Coulomb interactions on O $2p_\sigma$. We take a typical parameter set for cuprate superconductors [31]: $T_{pd} = 1$ eV, $T_{pp} = 0.3$ eV, $\Delta = 3$ eV, $U_d = 8$ eV, and $U_p = 4$ eV.

The dynamical charge structure factor on an orbital ϕ is given by

$$
N_\phi(\mathbf{q},\omega) = \sum_f |\langle f| N^\phi_\mathbf{q} |0\rangle|^2 \delta(\omega - E_f + E_0), \quad (1)
$$

where $|0\rangle$ and $|f\rangle$ represent the ground-state final state with energy E_0 and E_f, respectively, and $N^\phi_\mathbf{q}$ is the Fourier-transformed number operator on ϕ.

We perform a large-scale dynamical density-matrix renormalization-group (DMRG) calculation of $N_\phi(\mathbf{q},\omega)$ for a small system with $6 \times 4 = 24$ CuO$_2$ units, where a cylindrical
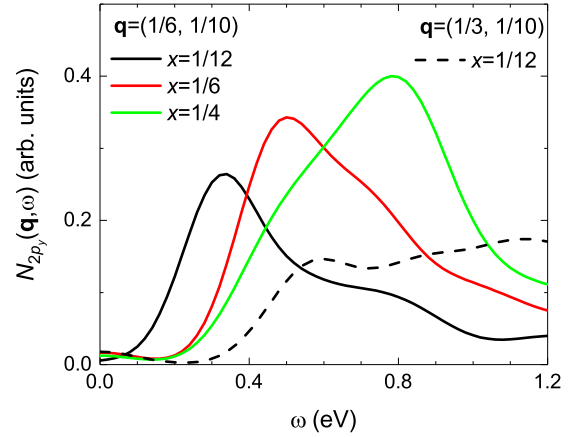
FIG. 3. Dynamical charge structure factor on O $2p_y$ orbital in a 6×4 cylindrical three-band Hubbard cluster with $T_{pd} = 1$ eV, $T_{pp} = 0.3$ eV, $\Delta = 3$ eV, $U_d = 8$ eV, and $U_p = 4$ eV. Black, red, and green solid lines represent spectra with hole concentration $x = 1/12$, $1/6$, and $1/4$, respectively, at **q** $= (1/6,1/10)$. Black broken line is for $x = 1/12$ at **q** $= (1/3,1/10)$. A Gaussian broadening width of 0.1 eV is used for the spectral weights. We note that small weights centered at $\omega = 0$ eV are due to less convergence in dynamical DMRG.

geometry with periodic (open) boundary conditions along the x (y) direction is introduced. In the cluster ($L_x = 6$ and $L_y = 4$), the x component of momentum **q** is determined by using a usual translational symmetry, i.e., $q_x = n_x/L_x$ ($n_x = 0, \pm 1, \pm 2, \ldots, L_x/2$ for the even number of L_x), but the y component is given by $q_y = n_y/(2L_y + 2)$ ($n_y = 1, 2, \ldots, L_y$) because of the open boundary condition. Defining l_x (l_y) as the x (y) component of the O $2p_y$ site l, we define the charge operator for $2p_y$ orbitals as

$$
N^{2p_y}_\mathbf{q} = \sqrt{\frac{2}{L_x(L_y + 1)}} \sum_l^L \sin(2\pi q_y l_y) e^{-i 2\pi q_x l_x} n_l,
$$

with n_l being the number operator at site l. We consider **q** with minimum q_y, i.e., $q_y = 1/10$, to make a comparison with the experimental data along the $(h,0)$ direction. Since the σ-polarized incident x-rays are employed in the experiments, the $1s$ core electron is excited to $2p$ orbitals perpendicular to the $(h,0)$ direction in the RIXS process, indicating predominant polarization for $2p_y$ orbitals. Therefore, we take $\phi = 2p_y$ in (1). See Appendix B for the details of the dynamical DMRG.

Figure 3 shows $N_{2p_y}(\mathbf{q},\omega)$ for hole concentrations $x = 1/12$, $1/6$, and $1/4$ at **q** $= (1/6,1/10)$ and for $x = 1/12$ at **q** $= (1/3,1/10)$. The broad peak shifts to higher energy with increasing x, accompanied by the increase of spectral weight. The peak positions at **q** $= (1/6,1/10)$ (0.3 eV at $x = 1/12$, 0.5 eV at $x = 1/6$, 0.8 eV at $x = 1/4$) are comparable to the experimental data near **q** $= (0.16,0)$ [0.49 eV at $x = 0.075$ in Fig. 2(f), 0.69 eV at $x = 0.18$ in Fig. 2(i), 0.65 eV at $x = 0.25$ in Fig. 2(j)]. With increasing **q** from $q_x = 1/6$ to $1/3$, the spectral weight shifts to higher energy as expected. Since these momentum and doping dependences of $N_{2p_y}(\mathbf{q},\omega)$ are consistent with the experimental observation, we ascribe the dispersive mode to the intraband charge excitations.
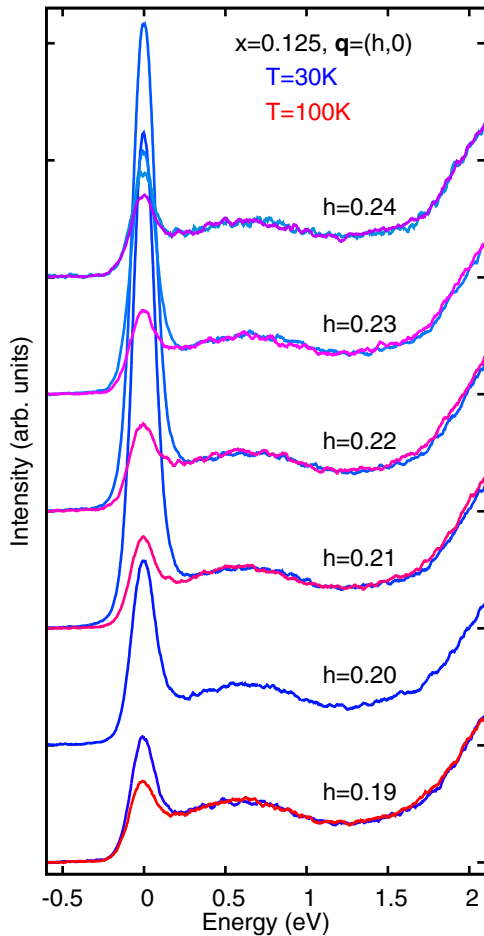
FIG. 4. Oxygen K-edge RIXS spectra of $La_{2-x}Ba_xCuO_4$ ($x = 0.125$) measured below (30 K) and above (100 K) the transition temperature of charge order ($T_{co} = 50$ K).

V. DISCUSSION

We have thus confirmed the presence of charge excitations, which are the counterpart of spin excitations, in the hole-doped cuprates by O K-edge RIXS. While the energy of the spin excitations (paramagnons) in LSCO is at most 0.3 eV [32–35], the charge excitations are observed up to 0.6–0.8 eV. These energy ranges of the excitations are reasonable because the magnitude of the dispersion of the spin and charge excitations are respectively scaled by the exchange interaction ($J \approx 0.1$ eV) and the transfer energy ($t \approx 0.4$ eV) in the terminology of the t-J model. The intraband charge excitations extend above 1 eV beyond the accessible Brillouin zone of the O K edge and the high-energy part of the excitations has been observed for overdoped compounds by Cu K-edge RIXS [10].

One may connect the charge excitations to the charge order, which has recently attracted great interest as a competing phenomenon to superconductivity [36–38]. We measured the oxygen K-edge RIXS spectra of LBCO $x = 0.125$ across the transition temperature of charge order at $T_{co} = 50$ K [39]. Figure 4 shows the spectra below (30 K) and above (100 K) T_{co}. The charge order is confirmed by the enhanced elastic scattering at 30 K. While the spin excitations might change slightly across the propagation vector of the charge order

[33], we could not find any change of the charge excitations across T_{co}. This may indicate that the effect of the charge order in hole-doped cuprates appears at lower energy than our experimental resolution. Judging from an optical study on the same material [40], the effect of the charge order on the electronic excitations would appear below 0.1 eV.

Combining the present work with the Cu L_3-edge RIXS of $Nd_{2-x}Ce_xCuO_4$ (NCCO) [14,15], we proved that momentum-dependent excitations at higher energy than spin excitations exist in both hole- and electron-doped systems. This strongly supports that the origin is charge excitations, which are common in the electron dynamics of doped Mott insulators. Because doped holes predominantly occupy the O $2p$ orbitals in the cuprates, the O K-edge RIXS represents a direct way to probe the charge dynamics of doped carriers and the intensity of charge excitations can be sizable. On the other hand, doped electrons are introduced to the upper Hubbard band of the Cu $3d$ orbital, and thus the Cu L_3-edge RIXS is sensitive to the charge excitations in the electron-doped cuprates. When compared quantitatively, the magnitude of the dispersion is larger in NCCO than in LSCO (LBCO), as shown in Figs. 2(g) and 2(h). Naively, the smaller charge-transfer gap of NCCO [41] gives a larger hopping energy, which agrees with the steeper dispersion, but more systematic studies on various cuprate superconductors are necessary to judge whether the sign of the charge of doped carriers is essential for the quantitative difference of the dispersion.

As shown in the spectra in this paper, the width of the charge excitations in the hole-doped cuprates is broader than the experimental resolution. This is also the case in the electron-doped cuprates. For example, the full width at the half maximum in NCCO $x = 0.15$ is 0.58 eV at $\mathbf{q} = (0.05,0)$ and $\mathbf{q} = (0.03,0.03)$ [14]. This broad line shape indicates that the charge excitations in this energy range are damped by the strong interaction between the charge, and it must be a common character in the doped Mott insulators. Furthermore, a slight shift of the peak position with changing E_i (nonperfect Raman behavior), shown in Fig. 1(c), suggests that the experimentally observed momentum-dependent feature is incoherent [12,42]. Then the feature comes from particle-hole charge excitations rather than coherent plasmon excitations.

VI. SUMMARY

We have performed an O K-edge RIXS study of $La_{2-x}(Br,Sr)_xCuO_4$ and identified the intraband charge excitations in the hole-doped cuprates. The charge excitations form a positive dispersing mode and the dispersion becomes steeper with increasing the hole concentration. Theoretical calculation of the dynamical charge structure factor on oxygen orbitals in a three-band Hubbard model agrees with the experimentally observed momentum and doping dependence. Our results confirm that the momentum-dependent charge excitations exist on the order of t, and the broad spectral line shape originating from the strong Coulomb interaction is a characteristic of the charge excitations in the doped Mott insulators. We conclude that identification of the spin and charge dynamics at the respective energy scale of J and t has been completed for both hole- and electron-doped cuprates.

APPENDIX A: MOMENTUM DEPENDENCE OF TWO-MAGNON EXCITATIONS

The momentum-dependent two-magnon excitations are calculated for the t-t'-t''-J model with a three-site term. The Hamiltonian is given by

$$H = H_{tt't''J} + H_{3s},$$

with

$$H_{tt't''J} = -t \sum_{\langle i,j \rangle_{1st},\sigma} (\tilde{c}_{i,\sigma}^\dagger \tilde{c}_{j,\sigma} + \text{H.c.})$$

$$- t' \sum_{\langle i,j \rangle_{2nd},\sigma} (\tilde{c}_{i,\sigma}^\dagger \tilde{c}_{j,\sigma} + \text{H.c.})$$

$$- -t'' \sum_{\langle i,j \rangle_{3rd},\sigma} (\tilde{c}_{i,\sigma}^\dagger \tilde{c}_{j,\sigma} + \text{H.c.}) + J \sum_{\langle i,j \rangle_{1st}} \mathbf{S_i} \cdot \mathbf{S_j}$$

and

$$H_{3s} = -\frac{J}{4} \sum_{\langle i,j \rangle_{1st}, \langle i,j' \rangle_{1st}, j \neq j', \sigma}$$

$$\times (\tilde{c}_{j',\sigma}^\dagger \tilde{n}_{i,-\sigma} \tilde{c}_{j,\sigma} - \tilde{c}_{j',\sigma}^\dagger \tilde{c}_{i,-\sigma}^\dagger \tilde{c}_{i,\sigma} \tilde{c}_{j,-\sigma} + \text{H.c.}),$$

where the summations $\langle i,j \rangle_{1st}$, $\langle i,j \rangle_{2nd}$, and $\langle i,j \rangle_{3rd}$ run over first, second, and third nearest-neighbor pairs, respectively. The operator $\tilde{c}_{i,\sigma} = c_{i,\sigma}(1 - c_{i,\sigma}^\dagger c_{j,\sigma})$ annihilates a localized electron with spin σ at site i with the constraint of no double occupancy, and $\mathbf{S}_i$ is the spin operator at site i. In the model, we set $t = 1$, $t' = -0.25$, $t'' = 0.12$, and $J = 0.4$. The real
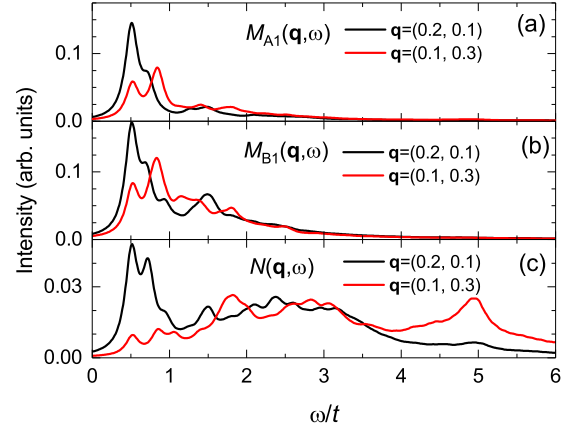

FIG. 5. The dynamical two-magnon correlation function for (a) A_1 mode, (b) B_1 mode, and (c) dynamical charge structure factor at $\mathbf{q} = (0.2, 0.1)$ (black solid line) and $(0.1, 0.3)$ (red solid line) for the $\sqrt{20} \times \sqrt{20}$ periodic cluster of the t-t'-t''-J model with three-site term: $t = 1$, $t' = -0.25$, $t'' = 0.12$, and $J = 0.4$. A Lorentzian broadening with a width of $0.2t$ is used for the spectral weights.

value of t in cuprate superconductors is usually taken to be 0.35 eV.

We define the momentum-dependent dynamical two-magnon correlation function as [12]

$$M_\pm(\mathbf{q},\omega) = \sum_f |\langle f|M_\mathbf{q}^\pm|0\rangle|^2 \delta(\omega - E_f + E_0), \quad \text{(A1)}$$

where $|0\rangle$ and $|f\rangle$ represent the ground and final states with energy E_0 and E_f, respectively, and $M_\mathbf{q}^\pm = \sum_\mathbf{k} (\cos k_x \pm \cos k_y)\mathbf{S_{k+q}} \cdot \mathbf{S_k}$. We note that $+$ $(-)$ corresponds to A_1 (B_1) representation and $\mathbf{S_k} = N^{-1/2} \sum_l e^{-i\mathbf{k}\cdot\mathbf{R}_l}\mathbf{S}_l$, with $\mathbf{R}_l$ being the position vector at site l and N being the total number of sites. Figures 5(a) and 5(b) show $M_+(\mathbf{q},\omega) = M_{A_1}(\mathbf{q},\omega)$ and $M_-(\mathbf{q},\omega) = M_{B_1}(\mathbf{q},\omega)$, respectively, at $\mathbf{q} = (0.2, 0.1)$ and $(0.1, 0.3)$ for a $N = \sqrt{20} \times \sqrt{20}$ periodic cluster with hole concentration $x = 2/20 = 0.1$. We find that the momentum dependence of spectral weight mainly appears only for the low-energy region less than $\omega = t = 0.35$ eV. This energy region is smaller than the region more than 0.4 eV, where the O K-edge RIXS has reported a dispersive mode, as shown in the main text. For comparison, the dynamical charge structure factor $N(\mathbf{q},\omega)$ is shown in Fig. 5(c). In contrast to the two-magnon excitations, momentum dependence appears even for the high-energy region up to $\omega \approx 6t \approx 2$ eV [14]. We note that $\mathbf{q} = (0.2, 0.1)$ and $(0.3, 0.2)$ are nearly the upper limit or higher than experimentally accessible momentum transfer.

APPENDIX B: DYNAMICAL DMRG CALCULATION OF DYNAMICAL CHARGE STRUCTURE FACTOR IN THE THREE-BAND HUBBARD MODEL

In calculating (1) by dynamical DMRG, we use a multitarget scheme and one of the targets, $(\omega - H + E_0 + i\gamma)^{-1}N_\mathbf{q}^{2p_y}|0\rangle$, is evaluated by using a kernel-polynomial

expansion method [43]. In our kernel-polynomial expansion method, the Lorentzian broadening with γ is replaced by a Gaussian broadening with half width at half maximum 0.1 eV. In our numerical calculations, we divide the energy interval from 0 to 1.2 eV by 61 mesh points and have targeted all of the points at once.

To perform DMRG, we construct a snakelike one-dimensional chain and use the truncation number $m = 2000$, and the resulting truncation error is less than 2×10^{-3}. In order to check the accuracy of our results, we examine the m dependence of $N_{2p_y}(\mathbf{q}, \omega)$. Figure 6 shows the results for hole concentration $x = 1/12$ at $\mathbf{q} = (1/6, 1/10)$. The difference between $m = 1500$ and $m = 2000$ is small near the peak position, though the convergence is not perfect at the higher energy region. Since it takes 24 hours by using 9600 nodes in the K computer, RIKEN Advanced Institute for Computational Science, to obtain a single curve of $N_{2p_y}(\mathbf{q}, \omega)$ with $m = 2000$ by our dynamical DMRG code, it is practically difficult to increase m further to perform systematic calculations of the doping and momentum dependence of dynamical charge structure factors.
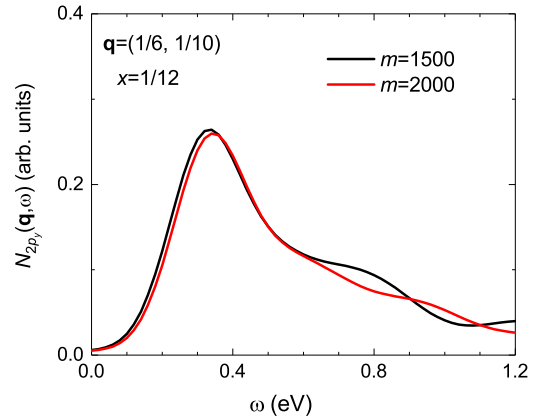

FIG. 6. The dependence of $N_{2p_y}(\mathbf{q}, \omega)$ for a given parameter set on the truncation number m in the dynamical DMRG method. A $6 \times 4 = 24$-unit cell CuO_2 cluster with cylindrical boundary condition is used. $\mathbf{q} = (6/6, 1/10)$. $T_{pp} = 0.3$ eV, $\Delta = 3$ eV, $U_d = 8$ eV, and $U_p = 4$ eV, and hole concentration $x = 1/12$. A Gaussian broadening with a width of 0.1 eV is used for the spectral weights.

[1] M. Imada, A. Fujimori, and Y. Tokura, Rev. Mod. Phys. **70**, 1039 (1998).

[2] P. A. Lee, N. Nagaosa, and X.-G. Wen, Rev. Mod. Phys. **78**, 17 (2006).

[3] B. Keimer, S. A. Kivelson, M. R. Norman, S. Uchida, and J. Zaanen, Nature (London) **518**, 179 (2015).

[4] L. J. P. Ament, G. Ghiringhelli, M. M. Sala, L. Braicovich, and J. van den Brink, Phys. Rev. Lett. **103**, 117003 (2009).

[5] L. Braicovich, J. van den Brink, V. Bisogni, M. M. Sala, L. J. P. Ament, N. B. Brookes, G. M. De Luca, M. Salluzzo, T. Schmitt, V. N. Strocov, and G. Ghiringhelli, Phys. Rev. Lett. **104**, 077002 (2010).

[6] S. Uchida, T. Ido, H. Takagi, T. Arima, Y. Tokura, and S. Tajima, Phys. Rev. B **43**, 7942 (1991).

[7] Y. Onose, Y. Taguchi, K. Ishizaka, and Y. Tokura, Phys. Rev. B **69**, 024504 (2004).

[8] Y.-J. Kim, J. P. Hill, S. Komiya, Y. Ando, D. Casa, T. Gog, and C. T. Venkataraman, Phys. Rev. B **70**, 094524 (2004).

[9] K. Ishii, K. Tsutsui, Y. Endoh, T. Tohyama, S. Maekawa, M. Hoesch, K. Kuzushita, M. Tsubota, T. Inami, J. Mizuki, Y. Murakami, and K. Yamada, Phys. Rev. Lett. **94**, 207003 (2005).

[10] S. Wakimoto, K. Ishii, H. Kimura, K. Ikeuchi, M. Yoshida, T. Adachi, D. Casa, M. Fujita, Y. Fukunaga, T. Gog, Y. Koike, J. Mizuki, and K. Yamada, Phys. Rev. B **87**, 104511 (2013).

[11] C. Jia, K. Wohlfeld, Y. Wang, B. Moritz, and T. P. Devereaux, Phys. Rev. X **6**, 021020 (2016).

[12] K. Tsutsui and T. Tohyama, Phys. Rev. B **94**, 085144 (2016).

[13] C. Monney, K. J. Zhou, H. Cercellier, Z. Vydrova, M. G. Garnier, G. Monney, V. N. Strocov, H. Berger, H. Beck, T. Schmitt, and P. Aebi, Phys. Rev. Lett. **109**, 047401 (2012).

[14] K. Ishii, M. Fujita, T. Sasaki, M. Minola, G. Dellea, C. Mazzoli, K. Kummer, G. Ghiringhelli, L. Braicovich, T. Tohyama, K. Tsutsumi, K. Sato, R. Kajimoto, K. Ikeuchi, K. Yamada,

M. Yoshida, M. Kurooka, and J. Mizuki, Nat. Commun. **5**, 3714 (2014).

[15] W. S. Lee, J. J. Lee, E. A. Nowadnick, S. Gerber, W. Tabis, S. W. Huang, V. N. Strocov, E. M. Motoyama, G. Yu, B. Moritz, H. Y. Huang, R. P. Wang, Y. B. Huang, W. B. Wu, C. T. Chen, D. J. Huang, M. Greven, T. Schmitt, Z. X. Shen, and T. P. Devereaux, Nat. Phys. **10**, 883 (2014).

[16] A. Greco, H. Yamase, and M. Bejas, Phys. Rev. B **94**, 075139 (2016).

[17] G. Ghiringhelli, A. Piazzalunga, C. Dallera, G. Trezzi, L. Braicovich, T. Schmitt, V. N. Strocov, R. Betemps, L. Patthey, X. Wang, and M. Grioni, Rev. Sci. Instrum. **77**, 113108 (2006).

[18] V. N. Strocov, T. Schmitt, U. Flechsig, T. Schmidt, A. Imhof, Q. Chen, J. Raabe, R. Betemps, D. Zimoch, J. Krempasky, X. Wang, M. Grioni, A. Piazzalunga, and L. Patthey, J. Synchrotron Radiat. **17**, 631 (2010).

[19] Y. Harada, M. Kobayashi, H. Niwa, Y. Senba, H. Ohashi, T. Tokushima, Y. Horikawa, S. Shin, and M. Oshima, Rev. Sci. Instrum. **83**, 013116 (2012).

[20] Y. Senba, S. Yamamoto, H. Ohashi, I. Matsuda, M. Fujisawa, A. Harasawa, T. Okuda, S. Takahashi, N. Nariyama, T. Matsushita, T. Ohata, Y. Furukawa, T. Tanaka, K. Takeshita, S. Goto, H. Kitamura, A. Kakizaki, and M. Oshima, Nucl. Instrum. Methods Phys. Res., Sect. A **649**, 58 (2011).

[21] M. Fujita, H. Goka, K. Yamada, and M. Matsuda, Phys. Rev. Lett. **88**, 167008 (2002).

[22] C. T. Chen, F. Sette, Y. Ma, M. S. Hybertsen, E. B. Stechel, W. M. C. Foulkes, M. Schluter, S.-W. Cheong, A. S. Cooper, L. W. Rupp, Jr., B. Batlogg, Y. L. Soo, Z. H. Ming, A. Krol, and Y. H. Kao, Phys. Rev. Lett. **66**, 104 (1991).

[23] Y. Harada, K. Okada, R. Eguchi, A. Kotani, H. Takagi, T. Takeuchi, and S. Shin, Phys. Rev. B **66**, 165104 (2002).

[24] V. Bisogni, L. Simonelli, L. J. P. Ament, F. Forte, M. Moretti Sala, M. Minola, S. Huotari, J. van den Brink, G. Ghiringhelli, N. B. Brookes, and L. Braicovich, Phys. Rev. B **85**, 214527 (2012).

[25] V. Bisogni, M. Moretti Sala, A. Bendounan, N. B. Brookes, G. Ghiringhelli, and L. Braicovich, Phys. Rev. B **85**, 214528 (2012).

[26] F. Forte, L. J. P. Ament, and J. van den Brink, Phys. Rev. B **77**, 134428 (2008).

[27] S. Sugai, S.-i. Shamoto, and M. Sato, Phys. Rev. B **38**, 6436 (1988).

[28] M. Rübhausen, C. T. Rieck, N. Dieckmann, K.-O. Subke, A. Bock, and U. Merkt, Phys. Rev. B **56**, 14797 (1997).

[29] J. G. Naeini, X. K. Chen, J. C. Irwin, M. Okuya, T. Kimura, and K. Kishio, Phys. Rev. B **59**, 9642 (1999).

[30] Y. Li, M. Le Tacon, Y. Matiks, A. V. Boris, T. Loew, C. T. Lin, L. Chen, M. K. Chan, C. Dorow, L. Ji, N. Barišić, X. Zhao, M. Greven, and B. Keimer, Phys. Rev. Lett. **111**, 187001 (2013).

[31] S. Maekawa, T. Tohyama, S. E. Barnes, S. Ishihara, W. Koshibae, and G. Khaliullin, *Physics of Transition Metal Oxides*, Springer Series in Solid-State Sciences Vol. 144 (Springer, Berlin, 2004), Chap. 2.

[32] M. P. M. Dean, G. Dellea, R. S. Springell, F. Yakhou-Harris, K. Kummer, N. B. Brookes, X. Liu, Y.-J. Sun, J. Strle, T. Schmitt, L. Braicovich, G. Ghiringhelli, I. Božvić, and J. P. Hill, Nat. Mater. **12**, 1019 (2013).

[33] M. P. M. Dean, G. Dellea, M. Minola, S. B. Wilkins, R. M. Konik, G. D. Gu, M. Le Tacon, N. B. Brookes, F. Yakhou-Harris, K. Kummer, J. P. Hill, L. Braicovich, and G. Ghiringhelli, Phys. Rev. B **88**, 020403(R) (2013).

[34] S. Wakimoto, K. Ishii, H. Kimura, M. Fujita, G. Dellea, K. Kummer, L. Braicovich, G. Ghiringhelli, L. M. Debeer-Schmitt, and G. E. Granroth, Phys. Rev. B **91**, 184513 (2015).

[35] C. Monney, T. Schmitt, C. E. Matt, J. Mesot, V. N. Strocov, O. J. Lipscombe, S. M. Hayden, and J. Chang, Phys. Rev. B **93**, 075103 (2016).

[36] J. M. Tranquada, B. J. Sternlieb, J. D. Axe, Y. Nakamura, and S. Uchida, Nature (London) **375**, 561 (1995).

[37] G. Ghiringhelli, M. Le Tacon, M. Minola, S. Blanco-Canosa, C. Mazzoli, N. B. Brookes, G. M. De Luca, A. Frano, D. G. Hawthorn, F. He, T. Loew, M. M. Sala, D. C. Peets, M. Salluzzo, E. Schierle, R. Sutarto, G. A. Sawatzky, E. Weschke, B. Keimer, and L. Braicovich, Science **337**, 821 (2012).

[38] R. Comin and A. Damascelli, Annu. Rev. Condens. Matter Phys. **7**, 369 (2016).

[39] M. Fujita, H. Goka, K. Yamada, J. M. Tranquada, and L. P. Regnault, Phys. Rev. B **70**, 104517 (2004).

[40] C. C. Homes, S. V. Dordevic, G. D. Gu, Q. Li, T. Valla, and J. M. Tranquada, Phys. Rev. Lett. **96**, 257002 (2006).

[41] Y. Tokura, S. Koshihara, T. Arima, H. Takagi, S. Ishibashi, T. Ido, and S. Uchida, Phys. Rev. B **41**, 11657(R) (1990).

[42] D. Benjamin, I. Klich, and E. Demler, Phys. Rev. Lett. **112**, 247002 (2014).

[43] S. Sota and T. Tohyama, Phys. Rev. B **82**, 195130 (2010).